International Journal of Thermophysics, Vol. 20, No. 4, 1999

Phase and Structural Modifications in Porous Silicon Under Pulse Heating[1]

L. N. Aleksandrov[2]

The phase transitions in crystalline and amorphous porous silicon layers on silicon single crystal under isothermal or laser pulse nanosecond heating were modeled. The pulse heating was described as an adiabatic process by using a quasi-statistical approximation through homogeneous nucleation and growth of a new phase. The calculation of the free energy of porous silicon for cylindrical, spherical, and complex structures of the pores and its dependence on the pore radius, overall porosity, and thermoelastic stresses was made. The equilibrium free energy increased to 0.15 and 0.09 eV, with a corresponding decrease in melting temperature of 400 and 300 K for crystalline and amorphous porous silicon, respectively. The Laplace pressure retards this shift no more than 10 K. The possibility of epitaxial silicon layer formation (0.1 to 1.2 μm thick) on porous silicon after pulse heating (30 ns; beam density from 2 to 10 $kJ \cdot m^{-2}$) is shown.

KEY WORDS: crystallization; isothermal heating; melting; phase diagram; porous silicon; pulse heating.

1. INTRODUCTION

Porous materials are of interest to science and technology due to their high surface area energy, absorption capacity, and optical and electrical properties. Since 1990, there has been a renewed interest in the study and application of silicon crystallites in the submicron nanometer range that are present

[1] Paper presented at the Fifth International Workshop on Subsecond Thermophysics, June 16–19, 1998, Aix-en-Provence, France.

[2] Institute of Semiconductor Physics, Academy of Science, Pr. Lavrentjeva 13, 630090 Novosibirsk, Russia.

0195-928X/99/0700-1223$16.00/0 © 1999 Plenum Publishing Corporation

in porous silicon (PS) [1]. The properties of PS are related to the number of pores and size distributions that determine the number and size of crystallites, the topological structure, and the total porosity. PS is usually formed by the anodic etching of a p-type silicon single-crystalline wafer in HF solution, but etching is also provided for amorphous silicon, obtained under deposition by ion implantation applied for doping. The sizes of pores cover four orders of magnitude: from 2 nm (nanopores) to 20 μm (macropores) in accordance with etching conditions and initial silicon properties. High-temperature treatment of PS is a component of technological processes under which it is used in microelectronics.

It was shown that annealing between 300 to 600°C induces a slight change in the PS structure [2]. Thermal treatment of PS for 30 min in the range of 400 to 900°C in vacuum and rapid thermal annealing (RTA) for 30 s (700 to 1200°C) were performed for photo- and electroluminescence intensity increase [3–6]. In these experiments porous surface passivation with oxygen and subsequent SiO_2 layer formation were shown. The possibility of crystallites and pore diameter changes for annealing temperatures above 500°C was pointed out in Refs. 3 and 4. The coalescence and densification of PS were observed by Labunov et al. [7] under heating at temperatures above 900°C, and after annealing in an H_2 atmosphere from 900 to 1200°C (for 30 min), the formation of spherical cavities and lattice deformation of 3×10^{-4} were noted. The problem of the structural stability and modification of PS under heating has attracted growing interest because of the use of PS layers as substrates for epitaxial Si deposition in SOI structures that may be effective only near 800°C [8].

The consideration of PS mechanical stability is connected with the specific surface area of a porous body and the high force per unit area on the capillary wall in contact with the environment that determine the action of local tensile stresses to 10 MPa [9]. Calculations showed an increase in lattice spacing a/a_0 of 10^{-4} and 10^{-2} for PS deposited on p-type Si [10]. The corresponding mechanical stresses in PS will have on effect on phase and structural transformations under heating. The use of computer simulation for the stress energy action analysis on structural changes in Si films under heating has been described by means of free energy changes and crystallization and melting kinetics calculations [11]. Numerical modeling to study the effect of the large surface area as a function of the pore size and configuration on the shifts of the melting temperature of crystalline and amorphous PS and on the kinetics of crystallization of amorphous PS was used. Isothermal heating was assumed, but the effect of mechanical stresses [12] was not taken into account. In the present work the melting of PS (crystalline or amorphous) and the crystallization of amorphous PS under isothermal or pulse heating are considered.

2. PHASE AND STRUCTURAL DIAGRAM OF POROUS SILICON

For the study of phase transitions in PS we determine the equilibrium phase diagram of state, free energy F–temperature T, including the effect of the pores and mechanical stresses. The free energy change $\Delta F_0(T)$ corresponds to bulk material. For $\Delta F_0(T)$ we used experimental data [13, 14] or the relationship

$$\Delta F_0(T) = \Delta H \, \Delta T / T_M \tag{1}$$

where T_M is the melting temperature (for the amorphous or crystalline phase), ΔH is the heat of melting, and $\Delta T = T - T_M$.

In order to calculate the additional free energy in porous materials, the total pore surface area was determined. Denoting the pore size distribution function as $f(r, h)$, the free energy per atom follows from the relationship

$$F_P(T) = F_0(T) + \Delta F_P = F_0(T) + B\sigma_{\alpha\beta} \int A(r, h) \, f(r, h) \, dr \, dh \tag{2}$$

where $A(r, h)$ is the surface area of a pore with radius r and height h, B is a normalizing factor, and $\sigma_{\alpha\beta}$ is the specific free energy at the interface between medium α and medium β.

For an estimation of the influence of the stress energy on the thermodynamics (and kinetics) of phase transitions, the relative lattice strain ε should be considered:

$$\Delta F_S = K_S \varepsilon^2 / 2 \tag{3}$$

where K_S is the elasticity modulus. Thus, the total $\Delta F_V = \Delta F_P(T) + \Delta F_S$. Equilibrium diagrams for crystal, liquid, and amorphous Si in (F, T) coordinates, shown in Fig. 1, were used to associate the increase in the free energy ΔF_V with the shift ΔT_M. For the C → L transition we use the relationship of similarity

$$\frac{T_M}{T_{MC} - T_{MA}} = \frac{F_V}{F_{CA}} \tag{4}$$

Here ΔF_{CA} is the free energy change under crystallization; the second subindex of T_M corresponds to the initial phase state. According to Eq. (4), ΔF_V for amorphous and crystalline states gives the shifts ΔT_{MA} and ΔT_{MC} of the melting points on the phase diagram.

In order to clarify the dependence of ΔF_P upon the pore radius r, idealized structures containing pores of the same shape and radius were

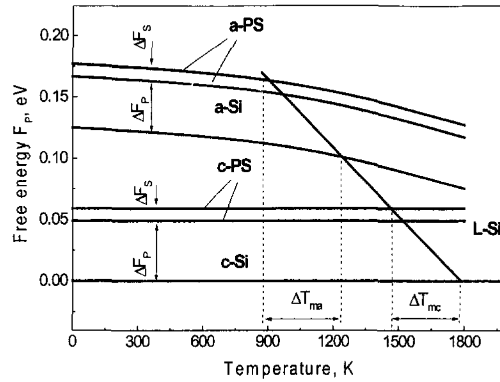

Fig. 1. Equilibrium diagram for crystalline and amorphous states of silicon in (F, T) coordinates [12, 14] and their modification for porous silicon (ΔF_P and ΔF_S values were calculated for cylindrical pores of radius 1 nm and $P=0.35$).

considered. Figure 2 illustrates schematically structures with (a) cylindrical and (b) spherical pores. For cylindrical pores with radius r_0 and height h_0:

$$A(r, h)=2\pi rh; \qquad f(r, h)=\delta(r-r_0)\,\delta(h-h_0)\,P/(\pi hr^2); \qquad \Delta F_P=2P\sigma_{\alpha\beta}/(n_0r_0) \tag{5}$$

For spherical pores with radius r_0:

$$A(r, h)=4\pi r^2; \qquad f(r, h)=3\delta(r-r_0)\,\delta(h-r_0)\,P/(4\pi r^3); \qquad \Delta F_P=3P\sigma_{\alpha\beta}/(n_0r_0) \tag{6}$$

where $\delta(x)$ is the Dirac delta function.

The porous structures obtained by computer simulation were presented in Ref. 12. The results of the two-dimensional model were extrapolated to the three-dimensional case, taking into account the axially symmetrical distribution of pores and their circular cross section in the plane normal to the direction of pore growth. The integral in Eq. (2) for this case was calculated numerically. A matrix of plane-parallel cross sections of simulated three-dimensional structures, as a function of depth ($h/h_{MAX}=0.15$ to 0.45) was obtained in Ref. 15. As in real structures, the change in porosity of PS with depth, must be taken into account in calculation of ΔF_P. For computing the crystal structure of PS, fractal dimensions were calculated.

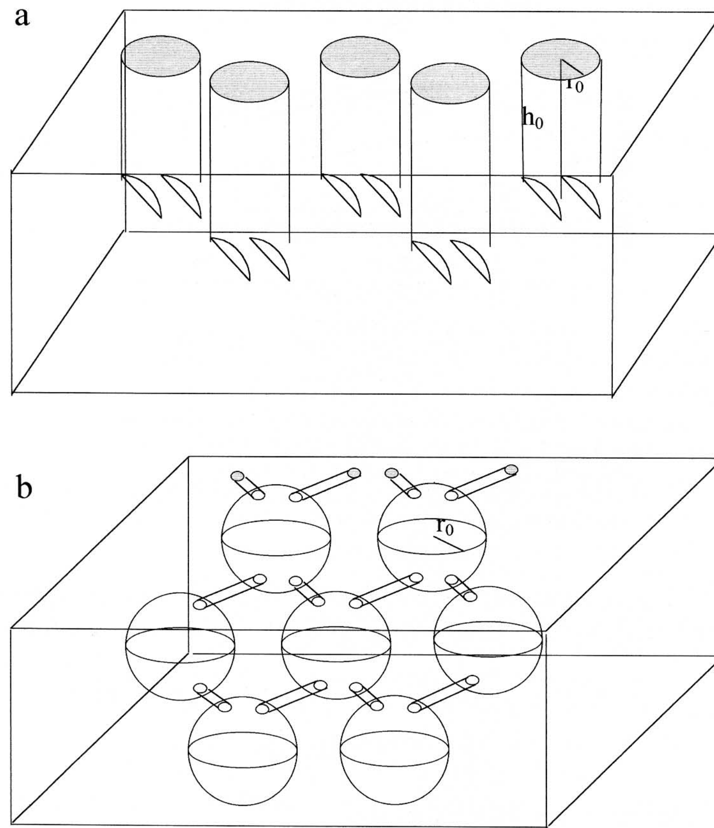

Fig. 2. Idealized pores structure with cylindrical (a) and spherical (b) pores.

They change from 0.1 to 3 in the range of sizes from 0.3 to 1 nm, which may be important for subnanoporous Si [16].

The difference between porous and nanostructural materials is manifested by the sign of the curvature radius $1/r_0$, which affects the value of T_M following from the P–T phase diagram in accordance with the Clapeyron–Clausius equation,

$$dT/dP = T(V_2 - V_1)/\Delta H_{12} \tag{7}$$

where V_1 and V_2 are the specific volumes of solid (A, C) and liquid phases, and ΔH_{12} is the heat of melting. For silicon, the volume change is negative under melting ($V_2 < V_1$), so the extreme Laplace pressure $\Delta P = \sigma_{12}/r_0$ at the surface of the nanoparticles accelerates melting but retards it at the pore surface.

3. SOLUTION OF THE THERMAL PROBLEM FOR PULSE HEATING

Short times involved in pulse annealing have provided new opportunities for structural modifications and phase transitions in thin films. If the pulse duration $\Gamma < t_0$, the induction period of transformation corresponds to the time for the appearance of the first nucleus and there will be no transformation. Pulse heating can cause superheating, following supercooling and various metastable solid structures [14]. A correlation was made between the diffusive length of heat conduction L during the action of the pulse and the near-surface layer thickness d_S, $L = (2a\Gamma)^{1/2}$, where a is the thermal diffusivity; thus, in crystalline PS for $\Gamma < 10$ ns, $L < 500$ nm and, in amorphous PS, nearly 100 nm [17]. Because of the low thermal conductivity of PS, heat exchange for $d_S < L$ with the environment does not occur and nanopulse heating proceeds adiabatically.

Melting of the PS layer (or part of the layer) without melting of the Si substrate is possible [18]. Computer simulation of Si surface heating, kinetics of melting, and crystallization under nanosecond pulses is presented in detail in Refs. 14 and 19. Under subsecond RTA of PS ($\Gamma > 0.1$ s) for $L > 0.5$ mm, the substrate has the same temperature as the surface region. For these isothermal conditions, melting of PS without substrate destruction is possible only due to their melting temperature differences. Under solid-state transformation the difference in thermal expansion coefficients of PS and Si creates thermoelastic stresses in PS, that affect melting kinetics or crystallization in amorphous PS. In the calculation of the temperature field and the melting-crystallization dynamics for laser pulse heating, we use the solution of Stefan's problem, including the thermal diffusion equation and the phase transition kinetic function $S(T, f)$ described in Refs. 14 and 19.

$$C(T, f)\, \partial T(r, t)/\partial r = \partial/\partial r[K_T(T, f)\, \partial T(r, t)/\partial r] + P(r, t, f) + Q(S)$$
$$Q(S) = \sum_{i=1}^{n} \Delta H v_i\, \delta(r - r_i) + q_i(S) \tag{8}$$

where $P(r, t, f)$ and $Q(S)$ are heat sources from absorbed radiation and phase transitions, $S(T, f)$ is the rate of the interface movement v_i and new interface formation by hetero- or homogeneous nucleation, and q_i is the heat from a critical nucleus. In accordance with the structure geometry, the solution of Eq. (8) is provided in one- or two-dimensional approximations; $C(T, f)$ and $K_T(T, f)$ are the heat capacity and thermal conductivity, respectively, and are functions of temperature and phase state. The absorption

of laser beam energy $P(r, t, f)$ in PS for a time t and energy density E has the form

$$P(r, t, f) = \frac{E}{\sqrt{\pi}} \beta \exp(-\beta(t - 1.2\Gamma)^2)(1 - R) \alpha \exp(-\alpha r) \tag{9}$$

where $\beta = 4 \ln 2/\Gamma^2$ and α is the coefficient of light absorption [19]. Modeling of the thermal annealing of a PS layer on single-crystalline Si shows the possibility of solid-phase crystallization of a-PS or melt-regrowth of a- or c-PS. If the pulse density $E < E_M$, which is necessary for melting of the entire PS layer h_{ps}, then $h_M < h_{PS}$, and crystallization of the melted part proceeds on the remaining part of the oriented crystalline PS, which is the well-known process of laser epitaxy for Si [20]. As shown in the first work on PS [18], these epitaxial films contained many dislocations and stacking faults, and for structure improvement, the covering of the PS surface with a-Si before heating was proposed [21].

4. KINETICS OF PHASE TRANSITIONS

The kinetics of phase transitions in Si is determined by three-dimensional nucleation and by growth of nuclei between pores or by two-dimensional nucleation of a new phase on the surface of the pores. We neglect the effect of stresses at the Si–SiO_2 interface that may occur on the pore surface due to possible oxidation. We assume that during crystallization, the shape and size of pores remain constant, since thermally induced modifications below 500°C do not change the microstructure of PS [2–4, 22].

The kinetics of the phase transition was described by the well-known time and temperature dependences of the transformed volume ratio, corresponding to a change of the parameters of the transition,

$$\eta(t) = 1 - \exp\left(-\int_0^t I_0(T)\, V(t-\tau)\, d\tau\right) \tag{10}$$

where I_0 and $V(t-\tau)$ are the nucleation rate and the volume of new phase centers, respectively. Equation (10) was originally used as a statistical probability model for the uncorrelated nucleation of a new phase in the transformed bulk [23]. It was shown later that the model is suitable for two-dimensional nucleus formation as well as for thin film deposition on a solid surface and recrystallization in thin layers [24]. The geometrical limitation of this model does not change its basic approximation [25], and analysis of experimental data relating to phase transformations in thin films

[26] makes it possible to use Eq. (10) to study the kinetic phase transitions in porous materials [12]. The relationships used for the calculation of I_0 and V are as follows.

For a quasi-spherical nucleus, $V = \pi r^2 a_0$ for two-dimensional ($n = 2$) and $V = 4\pi r^3/3$ for three-dimensional processes ($n = 3$).

$$r = C(t - \tau), \qquad C = C_0 \exp(-U/kT)[1 - \exp(-\Delta F_0/kT)]$$

$$I_0 = n_0 \nu \exp[-(W_c + U)/kT]$$

$$W_C = \pi a_0 \rho_c \sigma_{\alpha\beta}, \qquad \rho_c = \sigma_{\alpha\beta}/\Delta F_0 \qquad (n = 2)$$

$$W_C = 4\pi \rho_c^2 \sigma_{\alpha\beta} \Phi(\phi)/3, \qquad \rho_c = 2\sigma_{\alpha\beta}/\Delta F_0 \qquad (n = 3)$$

where $\Phi(\phi) = (1 - \cos\phi)^2 (2 + \cos\phi)/4$.

For three-dimensional nucleation on the surface, we use a contact angle of approximately 90° to determine $\Phi(\phi) \approx 1/2$. C is the growth rate, and $C_0 = 10^9$ cm $\cdot$ s^{-1}. This value was estimated using the experimental data of Lietoila et al. [27], t is the annealing time, $\sigma_{\alpha\beta}$ is the surface energy at the interface between medium α and medium β: σ_{cv} is for the crystal–vapor interface, σ_{cl} is for the crystal–liquid, σ_{al} is for the amorphous–liquid, and σ_{ac} is for the amorphous–crystal. The height of the monolayer is a_0, n_0 is the surface density of possible nucleation sites, ν is the atom oscillation frequency, U is the activation energy of a transition through the phase interface, ΔF_0 is the change in bulk free energy at the phase transition, and W_C is the work of formation of nuclei with critical radius r_0.

Melting is accelerated by decreasing r_C and W_C, as a result of an increase in ΔF_V. Unlike melting, for crystallization of amorphous material there is no definite phase transition temperature. It is necessary to study the kinetics of the A–C transformation. The shift of the crystallization kinetics may be determined by comparison of the $\eta(t, T)$ dependences in accordance with Eq. (10) for porous and bulk amorphous materials.

5. RESULTS AND DISCUSSION

In the calculation of thermodynamic parameters and phase transition kinetics in PS, data for bulk Si from Refs. 14, 28, and 29 and the latest experimental results for PS from Refs. 1, 30, and 31 were used. For a porosity P, the thermal conductivity is only $(1 - P)^{2/3}$ of the bulk value through the cross section and the specific volume is only $1 - P$ of the bulk value. Because of the density change, the specific heat and heat of melting must be estimated.

Table I. Values of Basic Parameters Used in the Calculations

Phase	K_T $(W \cdot K^{-1} \cdot m^{-1})$	C $(J \cdot K^{-1} \cdot m^{-3})$	a $(10^6 m^2 \cdot s^{-1})$	ρ $(Mg \cdot m^{-3})$	α $(10^6 m^{-1})$	R (%)	ΔH $(J \cdot m^{-3})$	$\sigma_{\alpha V}$ $(J \cdot m^{-2})$
Crystalline PS ($P=0.5$)	10	0.9	11	1.2	1.2	3	2.05	0.7
Amorphous PS ($P=0.5$)	0.3	1.0	0.3	1.1	21	2	1.6	0.6
Liquid	50	3.1	17	2.5	100	72		

The specific surface energy $\sigma_{\alpha\beta}$ is not known for the surface inside the pores, and its value varies from $0.2 \cdot Jm^{-2}$ for $c-l$ to $1 \ J \cdot m^{-2}$ for $c-v$. Values for PS, used in the calculations, are given in Table I.

The results obtained for ΔT_M versus the sizes of the cylindrical pores in crystalline PS for various porosities are presented in Fig. 3. For a pore size of 1 nm and a porosity of 0.35 (corresponds to values in Fig. 1), ΔT_{MC} is as much as 160 K. In spite of the lower value of the surface energy σ_{aV} compared to σ_{cV}, ΔT_{MA} is 40 K larger than ΔT_{MC}. For spherical pores, ΔF_V increases to 0.15 and 0.09 eV for crystalline and amorphous PS, ($r_0 = 1$ nm, $P = 0.52$) and the corresponding decrease in T_M is 400 and 300 K, respectively. The effect of thermoelastic stresses on ΔF_V from Eq. (3) is

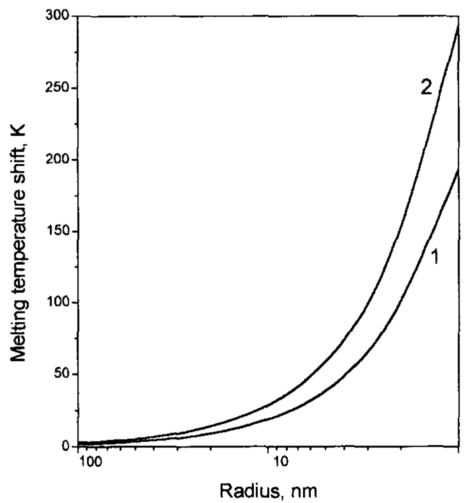

Fig. 3. Melting temperature shift ΔT_M for crystalline porous silicon versus radius of cylindrical pores for $P = 0.35$ (1) and $P = 0.52$ (2).

Table II. Results of Calculations of ΔF_P and ΔT_M for Porous Silicon

Pore shape	r_0 (nm)	P (%)	ΔF_P (eV)		ΔT_m (K)	
			Crystal	Amorphous	Crystal	Amorphous
Cylinder	1	35	0.059	0.053	268	265
Sphere	1	52	0.137	0.117	580	560
"Factal"	—	52	0.061	0.055	277	274

less than 0.01 eV ($\varepsilon < 0.001$). Table II presents the results obtained for cylindrical, spherical, and complex-shaped pores.

The results presented above are obtained under the assumption that the pores do not change their size before melting. In fact, under heating above 700 K, sintering above 1200 K [7] may cause an increase in the size of pores, which probably decreases the expected shift of melting temperature values. For solid-state crystallization the combination of different mechanisms of nucleation and growth is possible, including two- and three-dimensional processes. The crystallization occurs in the nanostructural amorphous phase between the pores, where the two-dimensional kinetics is favorable. The basic parameters are $a_0 = 0.25$ nm, $n_0 = 10^{19}$ m^{-2}, $\nu = 10^{13}$ s^{-1}, and $U = 2$ eV.

The calculation of the crystallization kinetics by Eq. (10), with $n = 2$, results in conventional S-type dependences upon T [23–26], which are shifted to low temperatures with a decrease in pore size because of the increasing specific area of the active surface of amorphous porous material (Fig. 4). For the melting process, the crystallization of a-PS with $r_0 < 10$

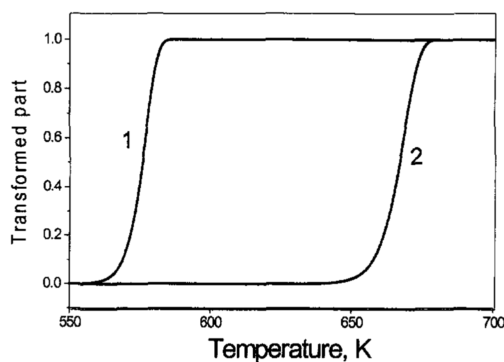

Fig. 4. Temperature dependence of the crystallized part of porous (1) and bulk (2) amorphous silicon ($t = 30$ min).

nm is strongly accelerated due to the effect of the free surface. Under this condition the specific surface area is a factor of 10^6 larger than that for bulk material, enhancing the two-dimensional nucleation of crystallites. The same shifts of kinetic curves of crystallization in a-PS as under isothermal (30-min) annealing are present under RTA ($T_{MAX} = 1000$ K, $t = 1$ s) because equivalent thermal budget of annealing is created in accordance with Eq. (7). Under nanopulse heating of PS, the thickness of the heat adsorbed layer $h_a = 1/\alpha$, which is up to 800 nm for crystalline PS, is up to 50 nm for a-PS. As mentioned above, for laser epitaxy and SOI structures of the Si–PS–epi-Si type, the melted layer thickness h_m must be less than h_{PS}. The results of calculations of the dependence of the maximum melting depth h_m on the beam energy density E [ruby laser, $\Gamma = 30$ ns (1), 300 ns (2), initial temperature $T_S = 300$ K] are shown in Fig. 5. For E from 2 to 10 $kJ \cdot m^{-2}$ (30 ns) on a PS formed single-crystalline Si layer with a thickness from 0.1 to 1.2 μm, the dependence in Fig. 5 is correlated with results from Ref. 18. For T_S to 500–800 K, the dependence of $h_m(E)$ shifts to lower E values. The detailed mechanism of Si epitaxial layer formation on PS is discussed in Refs. 32–34.

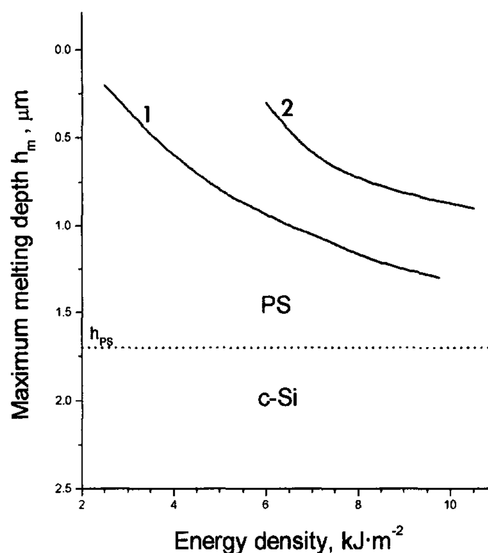

Fig. 5. Dependence of the maximum melting depth h_m of crystalline porous silicon as a function of energy beam density at pulse durations of 30 ns (1) and 300 ns (2); $T_S = 300$ K.

6. CONCLUSION

The analysis of both the porous and the nanostructural material properties shows that an increase in the specific surface area leads to a considerable increase in the surface free energy and, consequently, in the total free energy. The mechanical stresses in porous materials have relatively small effects on phase transitions under heating. In PS we have shifts of the equilibrium phase transition temperature from 100 to 400 K and acceleration of the crystallization kinetics in the amorphous phase under isothermal and pulse annealing. The melting of the subsurface layer in PS under pulse heating creates epitaxial regrowth of Si- and SOI-type structure formation. The effect was shown to be most significant for porous structures with $r_o < 10$ nm.

REFERENCES

1. P. M. Fauchet, J. von Behren, K. D. Hirschman, L. Tsybeskov, and S. P. Duttagupta, *Phys. Stat. Solidi A* **165**:3 (1998).
2. R. Herino, A. Perio, K. Barla, and G. Bomchil, *Mater. Lett.* **2**:519 (1984).
3. F. Moller, M. Ben Chorin, and F. Koch, *Thin Solid Films* **255**:16 (1995).
4. N. Hadj Zoubir, M. Vergnat, T. Delatour, A. Burneau, Ph. de Donato, and O. Barres, *Thin Solid Films* **255**:228 (1995).
5. W. Lange, P. Steiner, F. Kozlowski, and P. Ramm, *Thin Solid Films* **255**:224 (1995).
6. V. Petrova-Koc, T. Muschik, A. Kux, B. K. Meger, F. Koch, and V. Lehmann, *Appl. Phys. Lett.* **61**:943 (1992).
7. V. A. Labunov, V. P. Bondarenko, V. E. Borisenko, and A. M. Dorofeev, *Phys. Stat. Solidi A* **102**:193 (1987).
8. T. Yasumatsu, T. Ito, H. Nishizawa, and A. Hiraki, *Appl. Surf. Sci.* **48/49**:414 (1991).
9. U. Gruning and A. Yelon, *Thin Solid Films* **255**:135(1995).
10. M. Yang, D. Huang, P. Hao, F. Zhang, X. Hou, and X. Wang, *J. Appl. Phys.* **75**:651 (1994).
11. L. N. Aleksandrov, in *Polycrystalline Semiconductors*, Proc. Phys., Vol. 35 (Springer, Berlin, 1989), pp. 270–282.
12. L. N. Aleksandrov and P. L. Novikov, *Phys. Stat. Solidi A* **158**:419 (1996).
13. F. Spaepen and D. Turnbull, in *Laser Annealing in Semiconductors* (Academic Press, New York, 1982), p. 15.
14. L. N. Aleksandrov, *Progr. Crystal Growth Charact. Mater.* **24**:53 (1992).
15. L. N. Aleksandrov and P. L. Novikov, *Thin Solid Films* **330**:102 (1998).
16. L. N. Aleksandrov and P. L. Novikov, *Comput. Mater. Sci.* **10**:406 (1998).
17. G. Gasele, J. Linsmeier, V. Drach, J. Fricke, and R. Arensfischer, *J. Phys. D Appl. Phys.* **30**:2911 (1997).
18. H. Baumgart, R. C. Frey, F. Philip, and H. J. Leamy, in *Comparison of Thin Film Transistor and SOI Technologies*, H. W. Lam and M. J. Thompson, eds. (Elsevier, Amsterdam, 1984), pp. 63–68.
19. L. N. Aleksandrov, V. Ju. Balandin, A. V. Dvurechenskii, and O. A. Kulyasova, *Thin Solid Films* **171**:235 (1989).
20. L. N. Aleksandrov, *Progr. Gryst. Growth Charact.* **9**:227 (1984).

21. Yu. A. Manzhosov, A. V. Dvurechenskii, and S. I. Romanov, Patent USSR No. 1637599 (Moscow, 1991).
22. A. Halimaoui, Y. Campidelli, A. Larre, and D. Bensahel, *Phys. Stat. Solidi B* **190**:35 (1995).
23. A. N. Kolmogorov, *Izv. Akad. Nauk SSSR Ser. Math.* **3**:355 (1937).
24. L. N. Aleksandrov, *Growth of Crystalline Semiconductor Materials on Crystal Surfaces* (Elsevier, Amsterdam–Oxford–New York–Tokyo, 1984), p. 215.
25. V. Z. Belenkii, *Geometrical Probability Models of Crystallization* (Nauka, Moscow, 1980).
26. L. N. Aleksandrov, *Kinetics of Crystallization and Regrowth of Semiconductor Films* (Nauka, Novosibirsk, 1985).
27. A. Lietoila, R. B. Gold, and J. F. Gibbons, *Appl. Phys. Lett.* **39**:810 (1981).
28. T. Ning and C. Hilsum (eds.), *Properties of Silicon, EMIS Data Review Series No. 4* (INSPEC, London–New York, 1988).
29. P. J. Timans, in *Advances in Rapid Thermal and Integrated Processing, NATO ASI Ser. E Appl. Sci. Vol. 118*, F. Rooseboom, ed. (Kluwer, Dordrecht–Boston–London, 1996), pp. 35–101.
30. G. Benedetto, L. Boarino, and R. Spagnolo, *Appl. Phys. A Mater. Sci. Process.* **65**:155 (1977).
31. S. Frohnhoff, R. Arens-Fischer, T. Heinrich, J. Fricke, M. Arntzen, and W. Theiss, *Thin Solid Films* **255**:115 (1995).
32. T. L. Lin, S. C. Chen, K. L. Wang, and S. Iyer, in *Semiconductor on Insulator and Thin Film Transistor Technology*, A. Chang, M. W. Geis, and L. Pfeifer, eds. (MRS, Pittsburgh, 1986), pp. 193–197.
33. L. N. Aleksandrov, P. L. Novikov, A. V. Dvurechenskii, and V. A. Zinovyev, in *Extended Abstracts Int. Conf. Porous Semiconduct. Sci. Technol.* (University of Valencia, Spain, 1998), pp. 123–124.
34. P. L. Novikov, L. N. Aleksandrov, A. V. Dvurechenskii, and V. A. Zinov'ev, *JETP Lett.* **67**:539 (1998).